

The Role of Quantum in Hybrid Quantum-Classical Neural Networks: A Realistic Assessment

Dominik Freinberger^{1*} and Philipp Moser¹

¹*Research Unit Medical Informatics, RISC Software GmbH,
Softwarepark 32a, Hagenberg, 4232, Upper Austria, Austria.

Contributing authors: dominik.freinberger@risc-software.at;
philipp.moser@risc-software.at;

Abstract

Quantum machine learning has emerged as a promising application domain for near-term quantum hardware, particularly through hybrid quantum-classical models that leverage both classical and quantum processing. Although numerous hybrid architectures have been proposed and demonstrated successfully on benchmark tasks, a significant open question remains regarding the specific contribution of quantum components to the overall performance of these models. In this work, we aim to shed light on the impact of quantum processing within hybrid quantum-classical neural network architectures through a rigorous statistical study. We systematically assess common hybrid models on medical signal data as well as planar and volumetric images, examining the influence attributable to classical and quantum aspects such as encoding schemes, entanglement, and circuit size. We find that in best-case scenarios, hybrid models show performance comparable to their classical counterparts, however, in most cases, performance metrics deteriorate under the influence of quantum components. Our multi-modal analysis provides realistic insights into the contributions of quantum components and advocates for cautious claims and design choices for hybrid models in near-term applications.

Keywords: Quantum Machine Learning, Hybrid Quantum-Classical, Neural Networks, Medical Data

1 Introduction

Quantum machine learning (QML) has generated considerable excitement as a potential pathway to leverage near-term quantum devices for practical applications [1, 2]. Quantum neural networks (QNNs), parameterized quantum circuits executed on quantum computers and trained by classical hardware [3], have emerged as particularly promising models due to a certain resilience to noise [4] and their structural similarities with classical neural networks (NNs) [5]. Despite these appealing features, current implementations of QNNs face critical limitations, primarily due to hardware constraints. Particularly severe is the limited number of qubits available on existing quantum devices (or simulatable classically) and the error accumulation as well as the barren plateau phenomenon in deep circuits[6], which restrict the ability to encode high-dimensional data directly into QNNs.

To address these constraints, hybrid quantum-classical neural networks (HQNNs) have been proposed. HQNNs integrate QNNs into conventional NN architectures and are frequently explored for their promise of combining the strengths of both paradigms. NNs often act as initial feature extractors, producing fewer but highly informative latent features to be encoded into the QNN. The QNN is claimed to offer benefits including improved expressivity and training ability [7], among others. Despite the widespread adoption of HQNNs and their successful demonstrations on benchmark [8, 9] and real-world tasks [10–12], a central question remains largely unaddressed or even overlooked: To what extent does the quantum component truly contribute to the overall hybrid model performance?

Recent studies have offered mixed results. Some literature suggested that specific hybrid quantum-classical models offer performance improvements, such as enhanced accuracy [12–15] particularly with fewer training data [11]. Other works remained more cautious, presenting hybrid models as a promising approach requiring further exploration and validation [8, 9]. Yet others have taken a more critical look at the contribution of quantum components in specific settings. For example, [16] compared a hybrid architecture that encodes features from a pre-trained classical encoder into a QNN with angle encoding, evaluating it against various classical baselines and other hybrid models with pre-trained classical components. They reported that the inclusion of quantum components did not yield improvements over fully classical models. Similarly, as part of a broader QML benchmark, [17] investigated the transformations induced by a particular HQNN architecture and found them to be qualitatively similar to those produced by a corresponding classical model.

Motivated by this gap and the lack of consensus in the current understanding, our study expands upon these studies by providing a comprehensive and rigorous statistical analysis to assess the impact of quantum processing within a broad range of common HQNN architectures. In contrast to prior work such as [16], we focus on fully hybrid training schemes where classical and quantum components are optimized jointly, rather than relying on pre-trained classical encoders or separate training stages. By systematically varying classical pre-processing complexity, latent space dimensionality, quantum encoding methods, and measurement strategies, we aim to compare the contributions of quantum versus purely classical components on the overall model

score. We evaluate hybrid models against fully classical counterparts across three distinct medical data modalities: One-dimensional ECG signals, two-dimensional breast ultrasound images and three-dimensional chest CT image data, which represent some of the most frequent data types, especially in healthcare applications.

The remainder of the paper is organized as follows. Section 2 details our methodological setup, including the datasets, the HQNN architecture as well as variations of the hybrid and classical models and the training and evaluation protocols. Section 3 presents our empirical findings across all configurations and datasets. Finally, Section 4 discusses the implications of our results and concludes the paper.

2 Methods

2.1 Datasets and Modalities

We focused on binary classification tasks across diverse real-world medical data modalities using three publicly available datasets: the 1D MIT-BIH Arrhythmia dataset (electrocardiogram recordings) [18, 19], the 2D BreastMNIST dataset (breast ultrasound images), and the 3D NoduleMNIST3D dataset (chest CT volumes), the latter two being part of the bigger MedMNIST collection [20]. Fig. 1 shows illustrative samples. The 1D MIT-BIH Arrhythmia dataset contains 105,026 annotated ECG recordings sampled at 360 Hz from 47 subjects. Each sample represents a 1-second cardiac cycle (360 features). We formulate a binary classification task distinguishing normal beats from arrhythmic episodes. The 2D BreastMNIST dataset comprises 780 grayscale breast ultrasound images labeled as benign or malignant, resized to 224×224 pixels with values normalized to $[-1, 1]$. For the 3D modality, we use NoduleMNIST3D, consisting of 1,633 CT scans ($64 \times 64 \times 64$ voxels) of pulmonary nodules classified as malignant or benign. No additional pre-processing was applied to this dataset.

We sampled 7,064 instances from the MIT-BIH dataset and created five cross-validation folds, ensuring no subject overlap between training and validation folds to prevent data leakage. Similarly, for the MedMNIST datasets we created five separate training and validation folds based on the provided training and validation split. All training and validation folds were balanced in terms of class distribution.

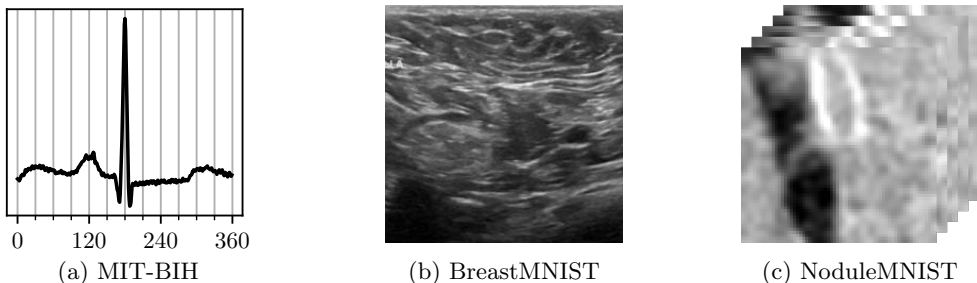


Fig. 1: Examples from the three datasets used in this study: 1D ECG (a), 2D breast ultrasound (b), and 3D chest CT (c).

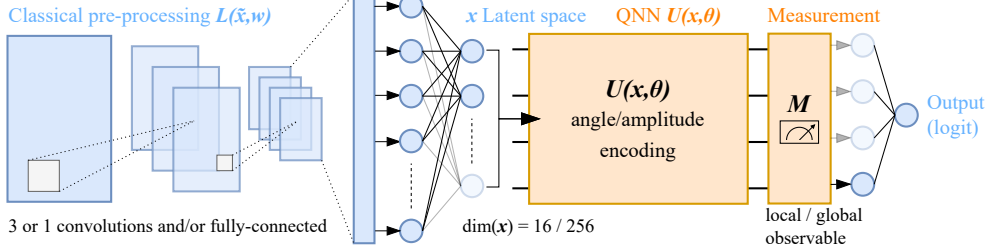


Fig. 2: Schematic illustration of the general HQNN architecture. A classical network $L(\tilde{\mathbf{x}}, \mathbf{w})$ (with 3, 1 or no convolutional layers) and a fully-connected layer (with or without $\pi \cdot \tanh$ activation) first extracts a latent feature vector \mathbf{x} (16 or 256 features). \mathbf{x} is then encoded into a quantum circuit $U(\mathbf{x}, \theta)$ using either angle or amplitude encoding (with optional entanglement). The expectation value of either a local or global Pauli-Z measurement is finally linearly mapped to the output logit.

2.2 Hybrid Model Architecture and Classical Reference

We adopted a prototypical hybrid model design inspired by [8]. The architecture comprised classical NN layers, $L(\tilde{\mathbf{x}}, \mathbf{w})$, pre-processing the raw input $\tilde{\mathbf{x}}$ into a latent feature representation \mathbf{x} . These features \mathbf{x} were given to the QNN $U(\mathbf{x}, \theta)$ for further processing. The QNN output, obtained by measuring an observable M , was post-processed by a linear fully-connected layer yielding the final logits. Fig. 2 illustrates this design. This architecture supports various input/output dimensions without constraints by the QNNs encoding capacity. Further, we isolated the contribution of the quantum circuit, by removing classical pre-processing stages or replacing the QNN entirely with classical layers. We implemented three variants of L , to systematically assess the influence of classical pre-processing:

- **3conv:** Three convolutional layers, each followed by Batch Normalization, ReLU activation, and Max-Pooling.
- **1conv:** A single convolutional layer with Batch Normalization, ReLU activation, and Max-Pooling.
- **0conv:** A single fully-connected layer without activation directly mapping the flattened input $\tilde{\mathbf{x}}$ to the latent representation \mathbf{x} .

Convolutional and pooling operations were adapted to the input dimensionality. The output from **3conv** and **1conv** was flattened before a final fully-connected layer produced the latent feature vector \mathbf{x} . We explored two latent dimensions: **16** and **256**. For angle-based feature encoding, we compared using a scaled activation function $\pi \cdot \tanh$ (mapping features to $[-\pi, \pi]$), versus no activation before the quantum encoding. For the QNN U , we used 4 or 8 qubits for latent dimensions **16** or **256**, respectively. We investigated four distinct QNN architectures, two using angle encoding and two using amplitude encoding:

- **Ang-RY:** The latent vector \mathbf{x} was partitioned into segments matching the number of qubits. Each segment was embedded using angle encoding via RY-rotations. These embedding layers alternated with variational layers comprising arbitrary single-qubit rotations followed by CNOT gates in a strongly entangling circular pattern. A final variational layer was applied after the last embedding layer. Although all latent features were encoded only once in the circuit, classical layers could have implicitly learned re-uploading important features [21].
- **Ang-Arb:** Similar to **Ang-RY**, but used arbitrary single-qubit rotations $R(\phi, \theta, \omega)$ around all axes to encode three features per gate. Variational layers also used arbitrary single-qubit rotations, with entanglement via CZ gates in an alternating nearest-neighbor pattern (even-indexed pairs 0-1, 2-3... were entangled first, then odd-indexed pairs 1-2, 3-4... were entangled in the next layer). This design was inspired by [5], adapted such that the latent feature vector was encoded once in the circuit, relying on classical layers to potentially learn data re-uploading as in the **Ang-RY** scheme. A final variational layer was applied.
- **Amp-Gen:** The normalized latent vector \mathbf{x} was embedded using amplitude encoding in a single step. This was followed by a variational layer structure identical to that in **Ang-RY**, including the strongly entangling circular pattern of CNOT gates and the final variational layer. This ensured that the number of variational layers (and therefore trainable parameters) was equal to the **Ang-RY** architecture.
- **QCNN:** Latent features \mathbf{x} were embedded using amplitude encoding. The **QCNN** architecture then utilized alternating quantum convolutional and pooling layers inspired by classical convolutional neural networks. Quantum convolution layers applied two-qubit unitary gates arranged in alternating pairings, first coupling even-indexed qubit pairs and then odd-indexed pairs with wrap-around connections. Quantum pooling layers reduced dimensionality by applying parameterized two-qubit unitary gates to pairs of qubits, effectively encoding the information into a single qubit per pair and subsequently disregarding one qubit, thus reducing the system's dimensionality. This procedure was repeated until a single output qubit remained, whose measurement determined the output [22, 23].

Motivated by prior findings [17] that entanglement may not improve performance, we compared circuits with and without entangling gates in the variational layers (except for **QCNN**, where entanglement is integral). The circuit output was the expectation value of one of two observables:

- **Local:** Separate Pauli-Z expectation values for each qubit.
- **Global:** Tensor product of Pauli-Z on all qubits, yielding the global observable $\bigotimes_{i=1}^N Z_i$.

The **QCNN** inherently used a single Pauli-Z measurement on the final qubit. Variational parameters were initialized from $\mathcal{N}(0, (0.01\pi)^2)$.

Classical reference models used identical pre-processing $L(\tilde{\mathbf{x}}, \mathbf{w})$ (**3conv**, **1conv**, **0conv**) and latent dimensions (**16**, **256**) as described above for the hybrid models as well as a final linear output layer. In place of the QNN, we evaluated four classical processing variations:

- **none**: Latent features were directly mapped to the output (via the linear post-processing layer).
- **fcnone**: A single hidden fully-connected layer (no activation).
- **fcrelu**: A single hidden fully-connected layer with ReLU activation.
- **mlp**: A multi-layer perceptron with three hidden fully-connected layers using ReLU activations.

2.3 Training and Statistical Evaluation

Models were trained using PyTorch [24]. Quantum circuits were simulated using PennyLane [25] with the ideal, noise-free `default.qubit` simulator. We used the Adam optimizer with binary cross-entropy loss with logits, a batch size of **256** for the 1D dataset and 64 for the 2D and 3D datasets, and a learning rate of 0.001. We employed a 5-fold cross-validation strategy as described in Section 2.1 for each model configuration and dataset. Performance was evaluated each epoch using ROC-AUC, average precision, and balanced accuracy. The best score for each metric within each fold was recorded, and results were averaged across the five folds to obtain a final score for each model configuration. Statistical significance was assessed using nonparametric tests (Wilcoxon signed-rank or Mann-Whitney U test, as appropriate) with Bonferroni correction for multiple comparisons, using a significance level of $\alpha = 0.05$.

3 Results

3.1 Influence of classical pre-processing layers

Across all data modalities, hybrid models exhibited considerably wider interquartile ranges in performance compared to purely classical models, often with significantly lower median ROC-AUC scores (Fig. 3). In the 1D and 2D datasets, the best-performing hybrid configurations achieved scores comparable to, or occasionally exceeding their classical counterparts (e.g., **Amp-Gen** with **0conv** pre-processing, latent dim. **16**, entanglement and **global** observable on the MIT-BIH data). Regarding the influence of classical pre-processing, we observed statistically significant differences between the **3conv** and **1conv** configurations ($p < 0.01$) as well as between the **3conv** and **0conv** configurations ($p < 0.001$) in the 2D setting. Similarly, in the 3D setting there was a significant difference ($p < 0.01$) between the **3conv** and **0conv** setting. This trend was less pronounced in the 1D dataset, where no significant difference in hybrid model performance was observed between the classical pre-processing configurations.

3.2 Influence of latent space dimension

We examined the impact of the latent feature space dimension on model performance in Fig. 4. For hybrid models, the smaller latent dimension of **16** generally led to higher median ROC-AUC scores compared to a larger dimension of **256**. This difference was most pronounced and statistically significant in the 1D case ($p < 0.001$). Across all modalities and both latent dimensions, the purely classical models consistently achieved significantly higher median performance than the hybrid models ($p < 0.001$).

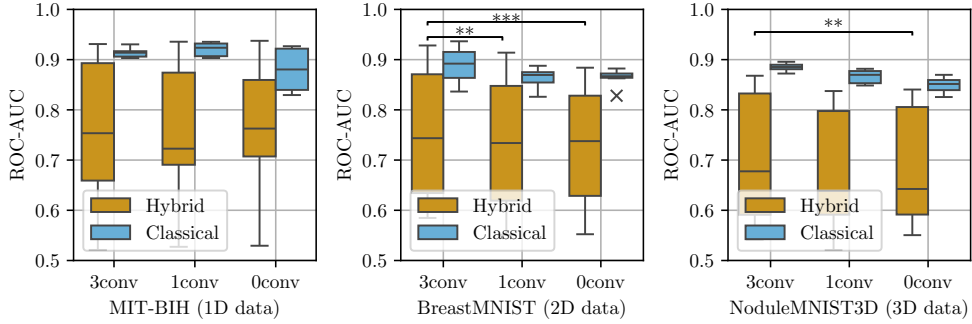


Fig. 3: Hybrid and classical model performances with different levels of classical pre-processing across data modalities. The influence of the pre-processing depth (3conv, 1conv, 0conv) is statistically compared between hybrid models and classical reference models (*: $p < 0.05$, **: $p < 0.01$, ***: $p < 0.001$).

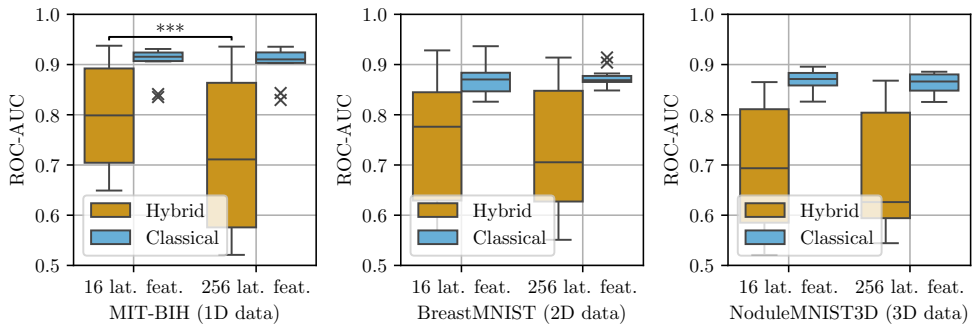


Fig. 4: Hybrid and classical model performances with different latent space dimensions across data modalities. The influence of the latent space dimension (16 vs. 256 features) is statistically compared between hybrid models and classical reference models (*: $p < 0.05$, **: $p < 0.01$, ***: $p < 0.001$).

in most comparisons). Among the classical models, the best results were obtained with **mlp** processing, **3conv** pre-processing, and **16** latent dim. for the 2D and 3D datasets, and with **fcrelu** processing, **1conv** pre-processing, and **256** latent dim. for the 1D dataset.

3.3 QNN architecture and feature encoding

Among the QNN architectures, amplitude encoding (**Amp-Gen**, **QCNN**) resulted in significantly higher median scores across all datasets compared to angle encoding (**Ang-RY**, **Ang-Arb**), as shown in Fig. 5. The **QCNN** architecture yielded the best median performance on 2D and 3D data. Notably, one specific configuration with angle encoding (**Ang-RY** with **3conv** pre-processing, **16** latent dim., entanglement

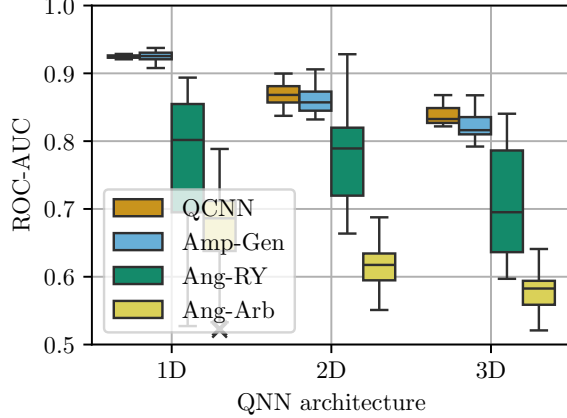


Fig. 5: ROC-AUC scores achieved by hybrid models, grouped by QNN architecture. Amplitude encoding models (**Amp-Gen**, **QCNN**) generally outperformed angle encoding models (**Ang-RY**, **Ang-Arb**).

and **global** observable) achieved the highest performance in the 2D dataset. The **Ang-Arb** architecture consistently performed the worst.

3.4 Latent layer activation function

For angle encoding models (**Ang-RY**, **Ang-Arb**), omitting the scaling activation function ($\pi \cdot \tanh$) before quantum encoding led to significantly better performance across all datasets (Fig. 6, left panel).

3.5 Entanglement in the variational circuit

Comparing models with (**ent.**) versus without entangling (**no ent.**) operations in the variational circuit (excluding **QCNN**), we observed a slight, nonsignificant trend towards better median performance when entanglement was present across all data modalities (Fig. 6, middle panel).

3.6 Type of observable

The choice of observable yielded different results depending on the encoding scheme (Fig. 6, right panel). For angle encoding models, using **local** Pauli-Z observables resulted in statistically significantly better median performance on 1D and 3D datasets compared to a **global** observable, with overall larger interquartile range. For amplitude encoding models (note: here only **Amp-Gen**, since **QCNN** uses a single local measurement by design), there was a nonsignificant trend favoring the **global** observable with higher median scores. Table 1 summarizes the performance across key metrics, comparing classical models against hybrid models grouped by QNN type.

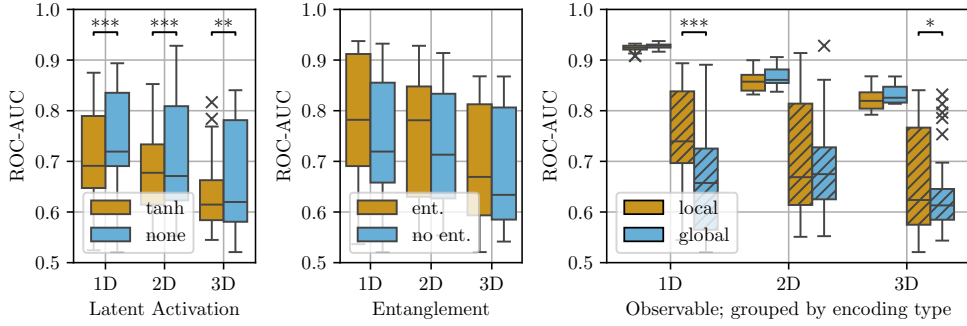


Fig. 6: Influence of quantum-specific hyperparameters on hybrid model performance. The impact of latent layer activation function, effect of entanglement and type of observable (here we additionally group by encoding type: striped boxplots represent angle encoding models) is statistically compared for all hybrid models (*: $p < 0.05$, **: $p < 0.01$, ***: $p < 0.001$).

Table 1: Performance metrics for classical and hybrid models.

Classical models are grouped together, hybrid models are split by QNN type. For each group the median score achieved is shown as well as minima and maxima in brackets. Bold highlights best median scores within each data modality.

| Dim. | Configuration | ROC-AUC | Avg. Precision | Balanced Acc. |
|------|---------------|-------------------------------------|-------------------------------------|-------------------------------------|
| 1D | Classical | 0.91 _[0.83, 0.94] | 0.90 _[0.81, 0.93] | 0.84 _[0.77, 0.86] |
| | Ang-RY | 0.80 _[0.53, 0.89] | 0.82 _[0.56, 0.90] | 0.70 _[0.50, 0.83] |
| | Ang-Arb | 0.69 _[0.52, 0.79] | 0.70 _[0.55, 0.77] | 0.59 _[0.50, 0.70] |
| | Amp-Gen | 0.93 _[0.91, 0.94] | 0.92 _[0.90, 0.94] | 0.85 _[0.74, 0.87] |
| | QCNN | 0.92 _[0.92, 0.93] | 0.92 _[0.91, 0.92] | 0.79 _[0.78, 0.82] |
| 2D | Classical | 0.87 _[0.83, 0.94] | 0.94 _[0.91, 0.97] | 0.83 _[0.77, 0.86] |
| | Ang-RY | 0.79 _[0.66, 0.93] | 0.92 _[0.85, 0.97] | 0.71 _[0.50, 0.86] |
| | Ang-Arb | 0.62 _[0.55, 0.69] | 0.82 _[0.77, 0.87] | 0.55 _[0.50, 0.65] |
| | Amp-Gen | 0.86 _[0.83, 0.91] | 0.94 _[0.93, 0.96] | 0.78 _[0.74, 0.83] |
| | QCNN | 0.87 _[0.84, 0.90] | 0.95 _[0.93, 0.96] | 0.77 _[0.75, 0.80] |
| 3D | Classical | 0.87 _[0.83, 0.90] | 0.78 _[0.75, 0.81] | 0.79 _[0.74, 0.81] |
| | Ang-RY | 0.70 _[0.60, 0.84] | 0.51 _[0.37, 0.74] | 0.55 _[0.50, 0.73] |
| | Ang-Arb | 0.58 _[0.52, 0.64] | 0.34 _[0.30, 0.40] | 0.51 _[0.50, 0.53] |
| | Amp-Gen | 0.82 _[0.79, 0.87] | 0.71 _[0.68, 0.78] | 0.70 _[0.54, 0.75] |
| | QCNN | 0.83 _[0.82, 0.87] | 0.72 _[0.71, 0.77] | 0.63 _[0.61, 0.68] |

4 Discussion

Hybrid quantum-classical neural networks (HQNNs) have gained considerable attention as promising near-term applications of quantum computing, particularly for processing high-dimensional data. Yet the specific contribution of their quantum components is often overlooked, with emphasis typically placed on overall model

performance. From our perspective, a more granular understanding of quantum contributions is crucial for advancing hybrid QML in a meaningful way. Motivated by this gap, our study systematically assessed the role of quantum processing within HQNNs across diverse real-world medical datasets, including 1D ECG signals, 2D breast ultrasound images, and 3D chest CT scans. The empirical findings offer a nuanced perspective on the contribution of quantum components to overall model performance.

Our results revealed that while some hybrid model configurations achieved scores comparable to classical counterparts, in most cases hybrid models underperformed relative to their classical references. This observation aligns with recent studies that found limited practical contributions of quantum components in hybrid quantum-classical configurations [16, 17]. Most hybrid models exhibited lower median performance and greater variability, indicating that simply incorporating quantum components into classical architectures does not inherently improve performance—and may even hinder it under certain conditions.

4.1 Influence of classical pre-processing layers

The extent of classical pre-processing had a significant effect on hybrid model performance. In the 2D and 3D datasets, performance improved with deeper classical feature extractors (**3conv** and **1conv**). While this trend was also observable in purely classical models, it was especially relevant for hybrid models, suggesting that quantum circuits alone might not efficiently handle high-dimensional feature extraction. The improved performance with deeper classical layers in higher-dimensional data (2D, 3D) suggests a greater need for classical pre-processing. However, as dimensionality does not equate to classification complexity, we avoid cross-dataset comparisons.

4.2 Influence of latent space dimension

We further observed that hybrid models benefited from higher classical compression, i.e., smaller latent spaces. This was particularly evident in the 1D dataset, where **256** latent features encoded into the quantum circuit led to significantly worse results than encoding just **16** features. Classical models, in contrast, were less sensitive to latent space size, further supporting the idea that quantum circuits struggle at extracting the most meaningful features [26]. These findings suggest either that increased classical processing improves performance (implying minimal quantum contribution), or that shallower quantum circuits learn more effectively, making overparameterization in quantum models less advantageous. Although we did not directly measure gradient variances in our experiments, barren-plateau theory predicts that gradient variance decays exponentially with both circuit depth and qubit count, leading to increased training difficulty for deeper models [6].

4.3 QNN architecture and feature encoding

Among the quantum-specific hyperparameters, the choice of encoding method had the most substantial impact. Across all modalities, amplitude encoding significantly outperformed angle encoding, a result consistent with prior studies on hybrid models

[27]. A possible explanation is given by [21], who prove that quantum models with angle encoding correspond to low-order Fourier series whose frequencies are determined by each single data upload, resulting in a restricted function class when features are uploaded only once in the circuit. To isolate the effect of the encoding scheme, we kept the number of qubits constant across both amplitude and angle encoding architectures. However, since angle encoding requires a number of encoding gates that scales linearly with the number of features (unlike the logarithmic scaling of amplitude encoding), we introduced additional encoding gates along the circuit to accommodate the full feature vector, as described in Section 2.2. This led to slightly increased circuit depth and complexity for angle encoding models, even though the number of qubits remained the same, which poses another possible reason for the worse performance of angle encoding models. Also, the incremental encoding scheme employed in both angle encoding models (**Ang-RY** and **Ang-Arb**) has led to mediocre results in earlier studies [26]. It should be noted, however, that amplitude encoding often requires complex state-preparation routines whose depth grows (in the worst case) exponentially with input dimension. As a result, the observed advantage may be offset by prohibitive circuit depth and gate counts on real NISQ hardware.

4.4 Latent layer activation function

In angle encoding models, applying a \tanh activation function (scaled to $[-\pi, \pi]$) prior to quantum encoding often led to worse performance compared to omitting activation altogether. While scaled activations are typically used to prevent ambiguity due to the periodic nature of rotation gates, they may also compress feature magnitudes too drastically, resulting in information loss. In contrast, allowing unbounded linear activations may risk exceeding the gate’s expected input range, but in practice, preceding classical layers appear to adapt to these constraints, a behavior observed previously [28].

4.5 Entanglement in the variational circuit

The inclusion of entanglement in the quantum circuits led to slightly higher median scores, although these differences were not statistically significant. This is reflected in contrasting literature: While some studies found that entanglement enhances expressivity and accuracy [29], others reported minimal or even negative effects [17], leaving the precise role of entanglement in HQNNs as an important open question for future research.

4.6 Type of observable

Local observables outperformed global observables predominantly within angle-encoding models. Conversely, amplitude-encoding models benefited more from global observables. A possible explanation is that amplitude encoding generates complex multi-qubit interactions to prepare a desired state which might be better captured by global observables. Additionally, prior work has found global observables to be more susceptible to barren plateaus [30], owing to vanishing gradients. However, our study did not directly measure gradient variances, so this remains a theoretical consideration.

4.7 Limitations

While our study investigated a broad range of representative HQNN architectures and quantum-specific hyperparameters, the design space of hybrid models remains vast. A comprehensive understanding of quantum contributions will require exploring an even wider spectrum of circuit topologies, integration strategies, and optimization methods beyond gradient-based training. Moreover, experiments used ideal, noise-free simulations, a simplification favoring quantum components, whereas real hardware noise will likely introduce additional challenges. We also limited our analysis to binary classification tasks, whereas quantum and hybrid models may prove more beneficial in alternative settings such as regression problems, unsupervised and reinforcement learning, or generative tasks.

5 Conclusion

In conclusion, this comprehensive empirical assessment contributes to the quantum machine learning discourse by providing clear insights into quantum components' contributions within hybrid models. While such hybrid models provide an attractive route to processing complex, real-world data, our work advocates for realistic expectations towards quantum utility and careful architectural decisions, as the overall benefit of quantum components remains nuanced and highly design- and data-dependent. Nonetheless, our study marks a meaningful empirical step toward practical quantum utility, helping to bridge the gap between theoretical promise and applied success. As quantum hardware and algorithms continue to evolve, future research building on these insights will be essential for objectively evaluating quantum computing's role in machine learning and artificial intelligence.

Statements and Declarations

Acknowledgements. This project is financed by research subsidies granted by the government of Upper Austria (MIMAS.ai) and by the FFG (QML4Med, grant no. 913256). www.ffg.at. RISC Software GmbH is a member of UAR (Upper Austrian Research) Innovation Network.

Competing interests. The authors declare that they have no known competing financial interests or personal relationships that could have appeared to influence the work reported in this paper.

Author contribution. Conceptualization: Dominik Freinberger, Philipp Moser; Methodology: Dominik Freinberger; Formal analysis and investigation: Dominik Freinberger; Writing - original draft preparation: Dominik Freinberger; Writing - review and editing: Dominik Freinberger, Philipp Moser; Funding acquisition: Philipp Moser; Resources: Philipp Moser; Supervision: Philipp Moser.

Data availability. All data used in this study are publicly available from open sources. Details on the datasets and how they were used are provided in the Methods section. The datasets can be accessed at the following URLs: [MIT-BIH Arrhythmia Database](#), [BreastMNIST](#) and [NoduleMNIST3D \(MedMNIST v2\)](#).

References

- [1] Cerezo, M., Verdon, G., Huang, H.-Y., Cincio, L., Coles, P.J.: Challenges and opportunities in quantum machine learning. *Nature Computational Science* **2**(9), 567–576 (2022) <https://doi.org/10.1038/s43588-022-00311-3> . Publisher: Nature Publishing Group. Accessed 2025-04-09
- [2] Wang, Y., Liu, J.: A comprehensive review of quantum machine learning: from NISQ to fault tolerance. *Reports on Progress in Physics* **87**(11), 116402 (2024) <https://doi.org/10.1088/1361-6633/ad7f69> . Publisher: IOP Publishing. Accessed 2025-04-09
- [3] Mitarai, K., Negoro, M., Kitagawa, M., Fujii, K.: Quantum circuit learning. *Physical Review A* **98**(3), 032309 (2018) <https://doi.org/10.1103/PhysRevA.98.032309> . Publisher: American Physical Society. Accessed 2025-04-11
- [4] Sharma, K., Khatri, S., Cerezo, M., Coles, P.J.: Noise resilience of variational quantum compiling. *New Journal of Physics* **22**(4), 043006 (2020) <https://doi.org/10.1088/1367-2630/ab784c> . Publisher: IOP Publishing. Accessed 2025-04-09
- [5] Pérez-Salinas, A., Cervera-Lierta, A., Gil-Fuster, E., Latorre, J.I.: Data re-uploading for a universal quantum classifier. *Quantum* **4**, 226 (2020) <https://doi.org/10.22331/q-2020-02-06-226> . Publisher: Verein zur Förderung des Open Access Publizierens in den Quantenwissenschaften. Accessed 2025-02-25
- [6] McClean, J.R., Boixo, S., Smelyanskiy, V.N., Babbush, R., Neven, H.: Barren plateaus in quantum neural network training landscapes. *Nature Communications* **9**(1), 4812 (2018) <https://doi.org/10.1038/s41467-018-07090-4> . Publisher: Nature Publishing Group. Accessed 2025-04-10
- [7] Abbas, A., Sutter, D., Zoufal, C., Lucchi, A., Figalli, A., Woerner, S.: The power of quantum neural networks. *Nature Computational Science* **1**(6), 403–409 (2021) <https://doi.org/10.1038/s43588-021-00084-1> . Publisher: Nature Publishing Group. Accessed 2025-04-11
- [8] Mari, A., Bromley, T.R., Izaac, J., Schuld, M., Killoran, N.: Transfer learning in hybrid classical-quantum neural networks. *Quantum* **4**, 340 (2020) <https://doi.org/10.22331/q-2020-10-09-340> . arXiv:1912.08278 [quant-ph]. Accessed 2025-03-17
- [9] Matic, A., Monnet, M., Lorenz, J.M., Schachtner, B., Messerer, T.: Quantum-classical convolutional neural networks in radiological image classification. In: 2022 IEEE International Conference on Quantum Computing and Engineering (QCE), pp. 56–66 (2022). <https://doi.org/10.1109/QCE53715.2022.00024> . <https://ieeexplore.ieee.org/document/9951255> Accessed 2025-03-21
- [10] Rainjonneau, S., Tokarev, I., Iudin, S., Rayaprolu, S., Pinto, K., Lemtiuzhnikova,

D., Koblan, M., Barashov, E., Kordzanganeh, M., Pflitsch, M., Melnikov, A.: Quantum Algorithms Applied to Satellite Mission Planning for Earth Observation. *IEEE Journal of Selected Topics in Applied Earth Observations and Remote Sensing* **16**, 7062–7075 (2023) <https://doi.org/10.1109/JSTARS.2023.3287154> . Conference Name: IEEE Journal of Selected Topics in Applied Earth Observations and Remote Sensing. Accessed 2025-03-10

[11] Sagingalieva, A., Kordzanganeh, M., Kenbayev, N., Kosichkina, D., Tomashuk, T., Melnikov, A.: Hybrid Quantum Neural Network for Drug Response Prediction. *Cancers* **15**(10), 2705 (2023) <https://doi.org/10.3390/cancers15102705> . Number: 10 Publisher: Multidisciplinary Digital Publishing Institute. Accessed 2025-03-10

[12] Xiang, Q., Li, D., Hu, Z., Yuan, Y., Sun, Y., Zhu, Y., Fu, Y., Jiang, Y., Hua, X.: Quantum classical hybrid convolutional neural networks for breast cancer diagnosis. *Scientific Reports* **14**(1), 24699 (2024) <https://doi.org/10.1038/s41598-024-74778-7> . Publisher: Nature Publishing Group. Accessed 2025-03-21

[13] Perelshtain, M., Sagingalieva, A., Pinto, K., Shete, V., Pakhomchik, A., Melnikov, A., Neukart, F., Gesek, G., Melnikov, A., Vinokur, V.: Practical application-specific advantage through hybrid quantum computing. *arXiv*. arXiv:2205.04858 [quant-ph] (2022). <https://doi.org/10.48550/arXiv.2205.04858> . <http://arxiv.org/abs/2205.04858> Accessed 2025-03-10

[14] Zeng, Y., Wang, H., He, J., Huang, Q., Chang, S.: A Multi-Classification Hybrid Quantum Neural Network Using an All-Qubit Multi-Observable Measurement Strategy. *Entropy* **24**(3), 394 (2022) <https://doi.org/10.3390/e24030394> . Number: 3 Publisher: Multidisciplinary Digital Publishing Institute. Accessed 2025-03-21

[15] Hafeez, M.A., Munir, A., Ullah, H.: H-QNN: A Hybrid Quantum–Classical Neural Network for Improved Binary Image Classification. *AI* **5**(3), 1462–1481 (2024) <https://doi.org/10.3390/ai5030070> . Number: 3 Publisher: Multidisciplinary Digital Publishing Institute. Accessed 2025-03-21

[16] Kölle, M., Maurer, J., Altmann, P., Sükel, L., Stein, J., Linnhoff-Popien, C.: Disentangling Quantum and Classical Contributions in Hybrid Quantum Machine Learning Architectures. *arXiv*. arXiv:2311.05559 [quant-ph] (2024). <https://doi.org/10.48550/arXiv.2311.05559> . <http://arxiv.org/abs/2311.05559> Accessed 2025-04-11

[17] Bowles, J., Ahmed, S., Schuld, M.: Better than classical? The subtle art of benchmarking quantum machine learning models. *arXiv*. arXiv:2403.07059 [quant-ph] (2024). <https://doi.org/10.48550/arXiv.2403.07059> . <http://arxiv.org/abs/2403.07059> Accessed 2025-03-12

[18] Goldberger, A.L., Amaral, L.A., Glass, L., Hausdorff, J.M., Ivanov, P.C., Mark,

R.G., Mietus, J.E., Moody, G.B., Peng, C.K., Stanley, H.E.: PhysioBank, PhysioToolkit, and PhysioNet: components of a new research resource for complex physiologic signals. *Circulation* **101**(23), 215–220 (2000) <https://doi.org/10.1161/01.cir.101.23.e215>

[19] Moody, G.B., Mark, R.G.: The impact of the MIT-BIH Arrhythmia Database. *IEEE Engineering in Medicine and Biology Magazine* **20**(3), 45–50 (2001) <https://doi.org/10.1109/51.932724>

[20] Yang, J., Shi, R., Wei, D., Liu, Z., Zhao, L., Ke, B., Pfister, H., Ni, B.: MedMNIST v2 - A large-scale lightweight benchmark for 2D and 3D biomedical image classification. *Scientific Data* **10**(1), 41 (2023) <https://doi.org/10.1038/s41597-022-01721-8>. Publisher: Nature Publishing Group. Accessed 2025-03-17

[21] Schuld, M., Sørensen, R., Meyer, J.J.: The effect of data encoding on the expressive power of variational quantum machine learning models. *Physical Review A* **103**(3), 032430 (2021) <https://doi.org/10.1103/PhysRevA.103.032430>. arXiv:2008.08605 [quant-ph]. Accessed 2025-02-26

[22] Cong, I., Choi, S., Lukin, M.D.: Quantum convolutional neural networks. *Nature Physics* **15**(12), 1273–1278 (2019) <https://doi.org/10.1038/s41567-019-0648-8>. Publisher: Nature Publishing Group. Accessed 2025-04-11

[23] Qiskit Community: Quantum Convolutional Neural Networks Tutorial. https://qiskit-community.github.io/qiskit-machine-learning/tutorials/11_quantum_convolutional_neural_networks.html. [Online; Accessed: Apr. 11, 2025]

[24] Paszke, A., Gross, S., Massa, F., Lerer, A., Bradbury, J., Chanan, G., Killeen, T., Lin, Z., Gimelshein, N., Antiga, L., Desmaison, A., Kopf, A., Yang, E., DeVito, Z., Raison, M., Tejani, A., Chilamkurthy, S., Steiner, B., Fang, L., Bai, J., Chintala, S.: PyTorch: An Imperative Style, High-Performance Deep Learning Library. arXiv. arXiv:1912.01703 [cs] (2019). <https://doi.org/10.48550/arXiv.1912.01703>. <http://arxiv.org/abs/1912.01703> Accessed 2025-04-14

[25] Bergholm, V., Izaac, J., Schuld, M., Gogolin, C., Ahmed, S., Ajith, V., Alam, M.S., Alonso-Linaje, G., AkashNarayanan, B., Asadi, A., Arrazola, J.M., Azad, U., Banning, S., Blank, C., Bromley, T.R., Cordier, B.A., Ceroni, J., Delgado, A., Matteo, O.D., Dusko, A., Garg, T., Gualà, D., Hayes, A., Hill, R., Ijaz, A., Isacsson, T., Ittah, D., Jahangiri, S., Jain, P., Jiang, E., Khandelwal, A., Kottmann, K., Lang, R.A., Lee, C., Loke, T., Lowe, A., McKiernan, K., Meyer, J.J., Montañez-Barrera, J.A., Moyard, R., Niu, Z., O’Riordan, L.J., Oud, S., Panigrahi, A., Park, C.-Y., Polatajko, D., Quesada, N., Roberts, C., Sá, N., Schoch, I., Shi, B., Shu, S., Sim, S., Singh, A., Strandberg, I., Soni, J., Száva, A., Thabet, S., Vargas-Hernández, R.A., Vincent, T., Vitucci, N., Weber, M., Wierichs, D., Wiersema, R., Willmann, M., Wong, V., Zhang, S., Killoran, N.: PennyLane: Automatic differentiation of hybrid quantum-classical computations. arXiv.

arXiv:1811.04968 [quant-ph] (2022). <https://doi.org/10.48550/arXiv.1811.04968> . <http://arxiv.org/abs/1811.04968> Accessed 2025-03-21

[26] Periyasamy, M., Meyer, N., Ufrecht, C., Scherer, D.D., Plinge, A., Mutschler, C.: Incremental Data-Uploading for Full-Quantum Classification. In: 2022 IEEE International Conference on Quantum Computing and Engineering (QCE), pp. 31–37 (2022). <https://doi.org/10.1109/QCE53715.2022.00021> . arXiv:2205.03057 [quant-ph]. <http://arxiv.org/abs/2205.03057> Accessed 2025-04-11

[27] Chen, Y., Griffin, P., Recchia, P., Zhou, L., Zhang, H.: Hybrid Quantum Neural Networks with Amplitude Encoding: Advancing Recovery Rate Predictions. arXiv. arXiv:2501.15828 [q-fin] (2025). <https://doi.org/10.48550/arXiv.2501.15828> . <http://arxiv.org/abs/2501.15828> Accessed 2025-04-10

[28] Lloyd, S., Schuld, M., Ijaz, A., Izaac, J., Killoran, N.: Quantum embeddings for machine learning. arXiv. arXiv:2001.03622 [quant-ph] (2020). <https://doi.org/10.48550/arXiv.2001.03622> . <http://arxiv.org/abs/2001.03622> Accessed 2025-04-10

[29] Nakhl, A.C., Quella, T., Usman, M.: Calibrating the role of entanglement in variational quantum circuits. Physical Review A **109**(3), 032413 (2024) <https://doi.org/10.1103/PhysRevA.109.032413> . arXiv:2310.10885 [quant-ph]. Accessed 2025-04-10

[30] Cerezo, M., Sone, A., Volkoff, T., Cincio, L., Coles, P.J.: Cost function dependent barren plateaus in shallow parametrized quantum circuits. Nature Communications **12**(1), 1791 (2021) <https://doi.org/10.1038/s41467-021-21728-w> . Publisher: Nature Publishing Group. Accessed 2025-04-11